Science AAAS

Electrically Induced Ferromagnetism at Room Temperature in Cobalt-Doped Titanium Dioxide

Y. Yamada, *et al.*

Science **332**, 1065 (2011);
DOI: 10.1126/science.1202152

This copy is for your personal, non-commercial use only.

If you wish to distribute this article to others, you can order high-quality copies for your colleagues, clients, or customers by clicking here.

Permission to republish or repurpose articles or portions of articles can be obtained by following the guidelines here.

The following resources related to this article are available online at www.sciencemag.org (this infomation is current as of October 16, 2011):

Updated information and services, including high-resolution figures, can be found in the online version of this article at:
http://www.sciencemag.org/content/332/6033/1065.full.html

Supporting Online Material can be found at:
http://www.sciencemag.org/content/suppl/2011/05/26/332.6033.1065.DC1.html

A list of selected additional articles on the Science Web sites **related to this article** can be found at:
http://www.sciencemag.org/content/332/6033/1065.full.html#related

This article **cites 20 articles**, 5 of which can be accessed free:
http://www.sciencemag.org/content/332/6033/1065.full.html#ref-list-1

This article has been **cited by** 1 articles hosted by HighWire Press; see:
http://www.sciencemag.org/content/332/6033/1065.full.html#related-urls

This article appears in the following **subject collections:**
Physics
http://www.sciencemag.org/cgi/collection/physics

Downloaded from www.sciencemag.org on October 16, 2011

Science (print ISSN 0036-8075; online ISSN 1095-9203) is published weekly, except the last week in December, by the American Association for the Advancement of Science, 1200 New York Avenue NW, Washington, DC 20005. Copyright 2011 by the American Association for the Advancement of Science; all rights reserved. The title *Science* is a registered trademark of AAAS.

Electrically Induced Ferromagnetism at Room Temperature in Cobalt-Doped Titanium Dioxide

Y. Yamada,[1]* K. Ueno,[2,3]* T. Fukumura,[3,4]† H. T. Yuan,[5,6] H. Shimotani,[5,6] Y. Iwasa,[5,6] L. Gu,[2] S. Tsukimoto,[2] Y. Ikuhara,[2,7,8] M. Kawasaki[1,2,5,6]

The electric field effect in ferromagnetic semiconductors enables switching of the magnetization, which is a key technology for spintronic applications. We demonstrated electric field–induced ferromagnetism at room temperature in a magnetic oxide semiconductor, $(Ti,Co)O_2$, by means of electric double-layer gating with high-density electron accumulation ($>10^{14}$ per square centimeter). By applying a gate voltage of a few volts, a low-carrier paramagnetic state was transformed into a high-carrier ferromagnetic state, thereby revealing the considerable role of electron carriers in high-temperature ferromagnetism and demonstrating a route to room-temperature semiconductor spintronics.

Magnetization of ferromagnetic materials is a fundamental quantity in various spintronic devices, such as magnetic random access memories. Magnetization control by electrical means is one of the central issues in semiconductor spintronics and will contribute to lower energy consumption of those devices (*1*, *2*). Ferromagnetic semiconductors possess both spin and charge degrees of freedom as a result of the carrier-mediated exchange interaction (*3*). Therefore, field-effect transistors made of ferromagnetic semiconductors are one of the most promising routes to realizing electrical control of magnetism, which in turn will lead to magnetization switching (*4*). In contrast, electric field control of ferromagnetic metals is limited to varying the magnetic anisotropy, which leads to magnetization rotation (*5*, *6*). The most well-studied ferromagnetic semiconductor, (Ga,Mn)As, has a Curie temperature (T_C) of 190 K (*7*), thus hindering the possibility of electrical control of ferromagnetism at room temperature.

The strong demand for higher-T_C ferromagnetic semiconductors led to the theoretical prediction of higher T_C in wide-gap magnetic semiconductors such as oxides (*8*). Subsequently, a combinatorial approach revealed that a magnetic oxide semiconductor, $(Ti,Co)O_2$, is ferromagnetic with $T_C > 400$ K (*9*). This compound exhibits the ferromagnetic magneto-optical effect and anomalous Hall effect at room temperature (*10*–*12*), thus satisfying important prerequisites to be classified as a ferromagnetic semiconductor (*3*). Electric field control of ferromagnetism should be possible at room temperature if ferromagnetism originates from a carrier-mediated mechanism.

The electric field effect has been used for transforming various electronic and magnetic phases in a wide range of materials (*4*, *13*). Usually, the accumulation of sufficiently high charge density ($>10^{14}$ cm^{-2}) to induce an exotic phase has been difficult because of dielectric breakdown of the gate insulator. Electric double layer transistors (EDLTs) have been developed as a powerful device structure allowing an extremely high electric field effect. EDLTs use a liquid electrolyte instead of a conventional solid gate insulator. Self-organized ions under an applied gate voltage form a nanometer-thick electric double layer to induce an image charge sheet on the channel surface, yielding a very high electric field on the order of 10 MV cm^{-1}.

Epitaxial films of anatase, $Ti_{0.90}Co_{0.10}O_2$ (001), were grown on $LaAlO_3$ (100) substrates by a pulsed laser deposition method (*14*). Bright-field scanning transmission electron microscopy (STEM) imaging and the corresponding energy-dispersive x-ray spectroscopy mapping for each constituent element (Fig. 1, A and B) reveal that Co atoms were distributed homogeneously inside the thin-film region without any segregation at the surface or interface, which is consistent with x-ray diffraction and atomic force microscopy analyses (*14*). In the atomically resolved high-angle annular dark-field STEM (HAADF-STEM) images (Fig. 1, D and E, for the regions indicated in Fig. 1C), the intensity of the atomic column is approximately proportional to the square of the atomic number (*15*). As shown in Fig. 1D, Ti atoms in the anatase TiO_2 buffer layer (upper part) were coherently grown on the $LaAlO_3$ substrate (bottom part), where bright and dark spots correspond to atomic columns of La and Al atoms, respectively. The anatase structure was coherently retained in the $Ti_{0.90}Co_{0.10}O_2$ film (Fig. 1E): The uniform contrast of Ti and Co atoms represents the homogeneous distribution of Co atoms substituting for Ti sites.

Figure 1F schematically shows the structure of an EDLT: A drop of electrolyte contacts the Hall bar channel and the Pt planar gate electrode (an optical microscope image is shown in fig. S1). We used two kinds of electrolyte (*14*). By applying a positive gate voltage, the cations and anions move to the channel and the gate electrode, respectively, and then an electric double layer is formed over the channel surface to accumulate electron carriers in the channel, leading to the emergence of ferromagnetism (Fig. 1G).

To probe the carrier accumulation and its ferromagnetic response, we carried out Hall effect measurements. The Hall resistivity (ρ_H) of $(Ti,Co)O_2$ can be expressed by the sum of the ordinary and anomalous Hall terms, $\rho_H = R_0H + R_S\mu_0M$, where R_0 and R_S are the ordinary and anomalous Hall coefficients, respectively; H is the magnetic field; μ_0 is the vacuum permeability and M is the magnetization (*16*). Accordingly; the anomalous Hall term can be an electrical probe of M and is useful particularly for thin films because of its small magnetization signal. The electron density n is inversely proportional to R_0, $n = (eR_0)^{-1}$, where e is the bare electron charge; the mobility μ can also be evaluated by measuring the resistivity (ρ_{xx}) according to the relation $\mu = R_0/\rho_{xx}$.

The blue curve in Fig. 1H is a transfer curve measured at 320 K for an EDLT with a 33-nm-thick $Ti_{0.90}Co_{0.10}O_2$ channel. The sheet conductance G_{xx} was enhanced above a gate voltage V_G of 3 V, indicating an electron channel field-effect transistor operation. The red circles in Fig. 1, H to J, respectively show G_{xx}, the sheet electron density (n_{2D}), and μ at 300 K measured during the temperature variation experiments (see Fig. 2A). The value of n_{2D} increased from 4.0×10^{13} cm^{-2} at $V_G = 0$ to 2.7×10^{14} cm^{-2} at $V_G = 3.8$ V, whereas μ remained almost constant. The maximum of the accumulated sheet electron density was as high as that observed in an EDLT using the same ionic liquid for gating (*17*). The value of G_{xx} at $V_G = 0$ was reproduced after repeated V_G scans. Hence, the enhancement in G_{xx} was caused by the electrostatic charge accumulation. Note that the extremely high chemical stability of $(Ti,Co)O_2$ prevented the films from undergoing electrochemical reactions during the repeated electric field effect measurements (*18*).

Figure 2A shows the temperature dependence of ρ_{xx} measured during cooling at various values of V_G. The charge accumulation transformed the channel from an insulative state to a metallic one. Shown in Fig. 2, B to D, are the values of conductivity (σ_{xx}), μ, and

[1]Institute for Materials Research, Tohoku University, Sendai 980-8577, Japan. [2]WPI-AIM Research, Tohoku University, Sendai 980-8577, Japan. [3]PRESTO, Japan Science and Technology Agency, Kawaguchi 332-0012, Japan. [4]Department of Chemistry, University of Tokyo, Tokyo 113-0033, Japan. [5]Quantum-Phase Electronics Center and Department of Applied Physics, University of Tokyo, Tokyo 113-8656, Japan. [6]CREST, Japan Science and Technology Agency, Tokyo 102-0075, Japan. [7]Institute of Engineering Innovation, University of Tokyo, Tokyo 113-8656, Japan. [8]Nanostructures Research Laboratory, Japan Fine Ceramics Center, Nagoya 456-8587, Japan.

*These authors contributed equally to this work.
†To whom correspondence should be addressed. E-mail: fukumura@chem.s.u-tokyo.ac.jp

Downloaded from www.sciencemag.org on October 16, 2011

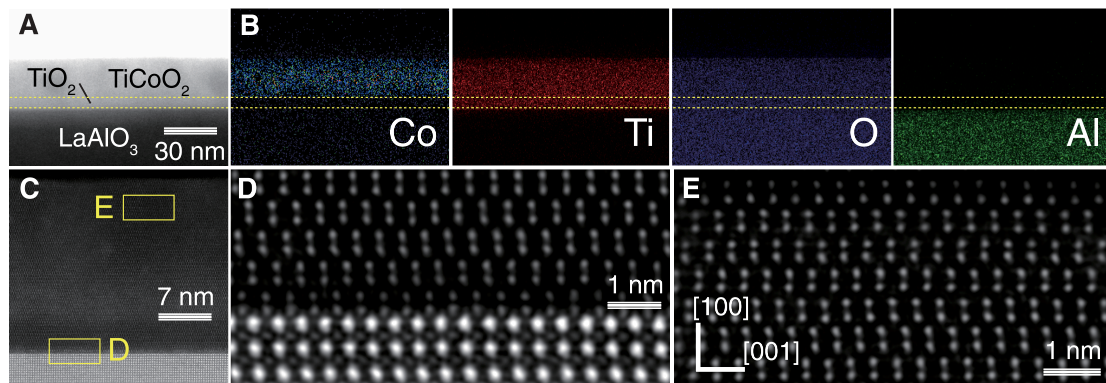

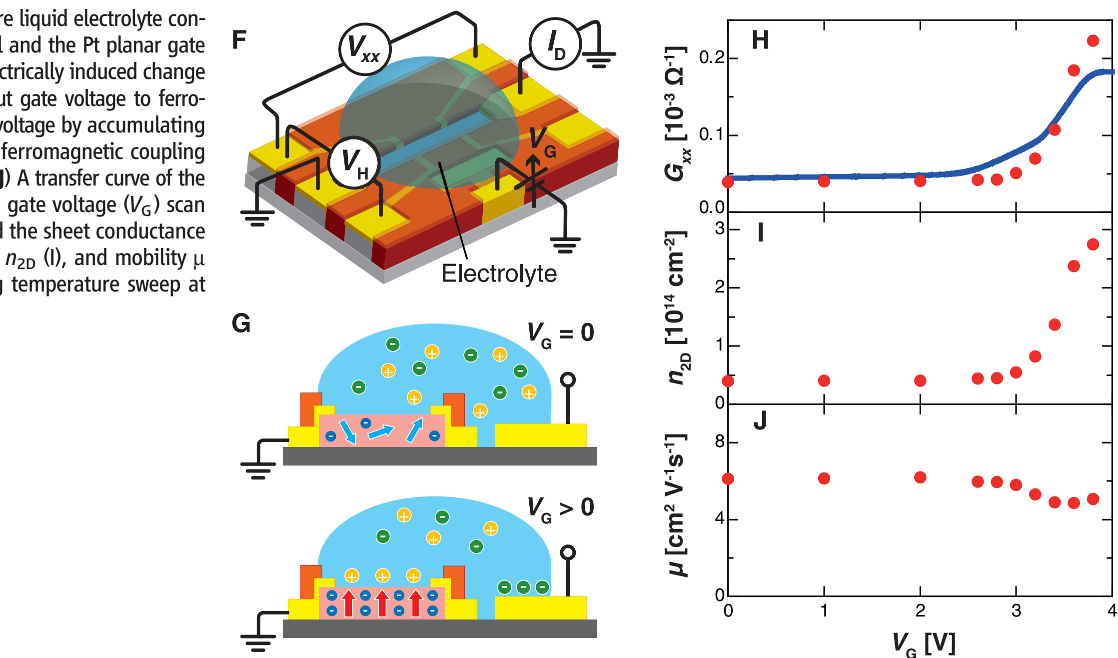

Fig. 1. (**A**) A bright-field STEM image of a $Ti_{0.90}Co_{0.10}O_2$ (001) / TiO_2 (001) / $LaAlO_3$ (100) substrate. (**B**) The corresponding energy-dispersive x-ray spectroscopy mappings for Co, Ti, O, and Al. (**C**) Cross section showing location of images in (D) and (E). (**D** and **E**) Atomically resolved high-resolution HAADF-STEM images at the TiO_2 / $LaAlO_3$ interface (D) and within the $Ti_{0.90}Co_{0.10}O_2$ film (E). (**F**) A schematic of an electric double layer transistor (EDLT), where liquid electrolyte contacts the $Ti_{0.90}Co_{0.10}O_2$ channel and the Pt planar gate electrode. (**G**) Illustration of electrically induced change from paramagnetic state without gate voltage to ferromagnetic state with finite gate voltage by accumulating electron carriers that mediate ferromagnetic coupling between localized spins. (**H** to **J**) A transfer curve of the EDLT at 320 K measured with a gate voltage (V_G) scan rate of 1 mV/s (blue curve) and the sheet conductance G_{xx} (H), sheet electron density n_{2D} (I), and mobility μ (J) at 300 K measured during temperature sweep at each V_G (red circles).

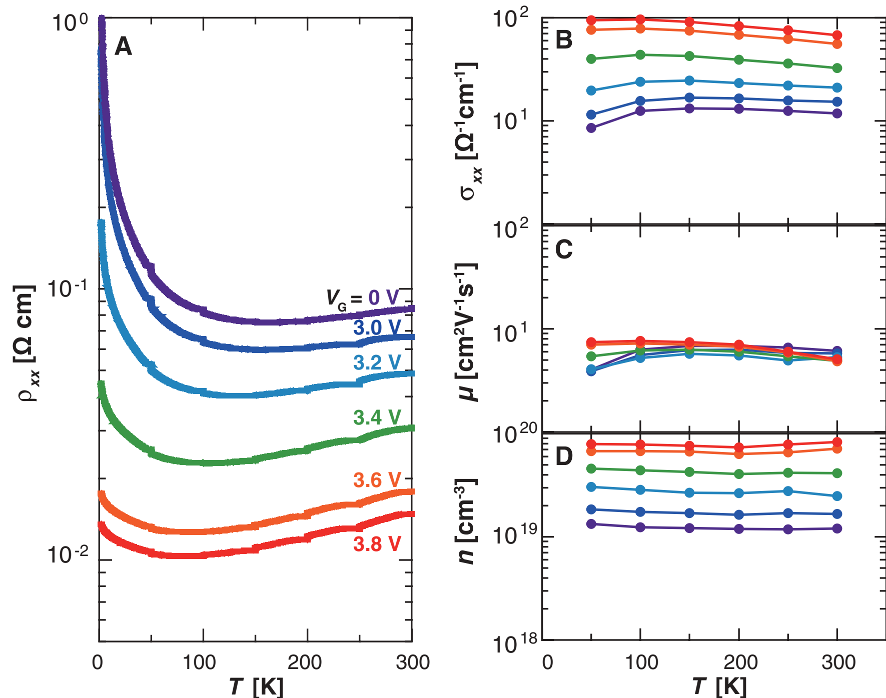

Fig. 2. (**A**) Temperature dependence of resistivity ρ_{xx} in $Ti_{0.90}Co_{0.10}O_2$ channel measured while cooling from 320 K with application of each gate voltage V_G. From 300 to 50 K in decrements of 50 K, the temperature was kept constant while the magnetic field was swept between +0.5 T and −0.5 T for the Hall effect measurements. (**B** to **D**) Temperature dependences of conductivity σ_{xx} (B), mobility μ (C), and electron density n (D) at each V_G; colors correspond to those in (A).

Downloaded from www.sciencemag.org on October 16, 2011

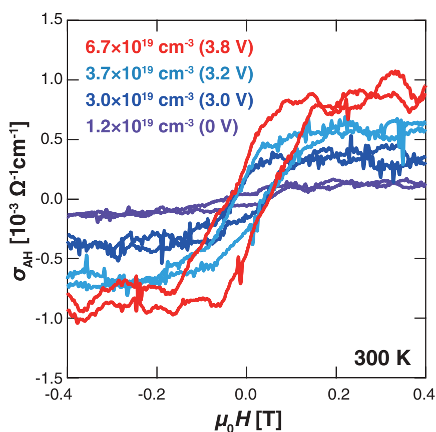

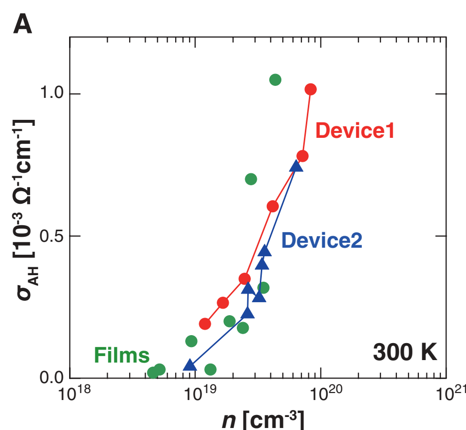

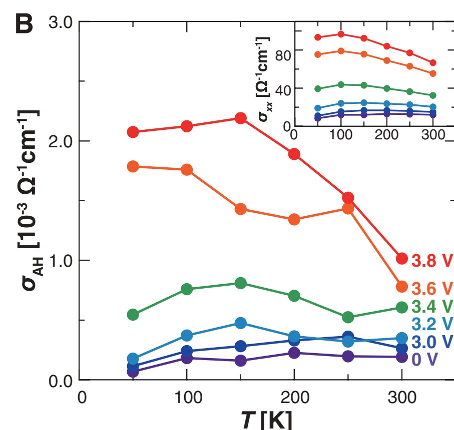

Fig. 3. Magnetic field ($\mu_0 H$, where μ_0 is the vacuum permeability) dependence of the anomalous Hall conductivity σ_{AH} at 300 K, measured at different gate voltages V_G. The values of electron density n at each V_G obtained from the ordinary Hall effect are shown in parentheses. The upper and lower curves for each color correspond to the anomalous Hall conductivity with decreasing and increasing magnetic field, respectively.

Fig. 4. (**A**) Relationship between anomalous Hall conductivity σ_{AH} and electron density n at 300 K. Red circles and blue triangles denote the data for two different EDLTs (devices 1 and 2, respectively). The applied gate voltage V_G was 0 to 3.8 V for device 1 and 0 to 3.75 V for device 2. Green circles denote the data from nine $Ti_{0.90}Co_{0.10}O_{2-\delta}$ samples, in which the electron density was varied by tuning the concentration of the oxygen vacancy δ. (**B**) Temperature dependence of the anomalous Hall conductivity for each gate voltage V_G. The inset shows temperature dependence of the longitudinal conductivity σ_{xx}, converted from Fig. 2B.

the volume electron density (n) evaluated from the ordinary part of the Hall resistance at each temperature, where n was obtained from n_{2D} divided by the film thickness, assuming a uniform distribution of electron density along the depth, for the sake of comparison with chemically doped samples. The increase in σ_{xx} was dominated by the increase in n.

Such a high-density accumulation of charge carriers had a striking effect on the magnetism at room temperature. Figure 3 shows the magnetic field dependence of anomalous Hall conductivity (σ_{AH}) at each V_G (*19*). At $V_G = 0$, σ_{AH} was almost negligible, indicating that the $Ti_{0.90}Co_{0.10}O_2$ channel was in a paramagnetic state. With increasing V_G, σ_{AH} was enhanced to show the clear emergence of hysteresis, indicating the electric field–induced ferromagnetic state.

The relationship between σ_{AH} and n at 300 K is summarized in Fig. 4A for the two different EDLTs (devices 1 and 2), superposed with the data from nine samples of chemically doped $Ti_{0.90}Co_{0.10}O_{2-\delta}$, in which the oxygen vacancy δ was varied as the electron donor. At $V_G = 0$ V, σ_{AH} was negligible in both devices. By accumulating n greater than ~1×10^{19} cm^{-3}, σ_{AH} was steeply increased by the emergence of the ferromagnetic state. These EDLT data showed good agreement with those of the chemically doped samples, plausibly ruling out extrinsic sources such as magnetic nanoparticles as a cause of the increased σ_{AH}, because the electric field changes only the amount of n. The temperature dependence of σ_{AH} at each V_G is shown in Fig. 4B. The amplitude of σ_{AH} was enhanced above V_G of 3.4 V at all temperatures. The inset in Fig. 4B shows the temperature dependence of σ_{xx}. Note that σ_{AH} and σ_{xx} show quite similar temperature dependence, indicating that the electrical conduction induced the ferromagnetic coupling.

The electrically induced ferromagnetism supports the idea that the ferromagnetism originates from a carrier-mediated mechanism (*20*) rather than a non–carrier-mediated one (*21*). The enhanced T_C with a positive V_G is consistent with the polarity of electron carriers, which are expected to mediate the exchange coupling, in contrast with hole carriers in (Ga,Mn)As (*22*). T_C inferred from Fig. 4B might not be a monotonically increasing function of the carrier density, in contrast to the carrier-mediated mechanism seen with (Ga,Mn)As. Thus, a more systematic study of T_C will be needed, with the change of V_G polarity and the temperature dependences, to elucidate the details of the carrier-mediated mechanism.

Our results show that ferromagnetism can be induced in low-carrier paramagnetic $Ti_{0.90}Co_{0.10}O_2$ with a huge amount of electron charge accumulation by using an EDLT geometry. This method offers promise for future semiconductor spintronics operating at room temperature, such as a gate-tunable magnetization inversion (*23*) and the gate-tunable magneto-optical effect (*10*). Such gate-tunable ferromagnetism will also contribute to manipulation of magnetic bits with lower dissipation than that achieved in ferromagnetic metal memories.

References and Notes

1. S. A. Wolf *et al.*, *Science* **294**, 1488 (2001).
2. I. Žutić, J. Fabian, S. Das Sarma, *Rev. Mod. Phys.* **76**, 323 (2004).
3. A. H. MacDonald, P. Schiffer, N. Samarth, *Nat. Mater.* **4**, 195 (2005).
4. H. Ohno *et al.*, *Nature* **408**, 944 (2000).
5. M. Weisheit *et al.*, *Science* **315**, 349 (2007).
6. T. Maruyama *et al.*, *Nat. Nanotechnol.* **4**, 158 (2009).
7. T. Dietl, *Nat. Mater.* **9**, 965 (2010).
8. T. Dietl, H. Ohno, F. Matsukura, J. Cibert, D. Ferrand, *Science* **287**, 1019 (2000).
9. Y. Matsumoto *et al.*, *Science* **291**, 854 (2001).
10. T. Fukumura *et al.*, *Jpn. J. Appl. Phys.* **42**, L105 (2003).
11. H. Toyosaki *et al.*, *Nature Mater.* **3**, 221 (2004).
12. K. Ueno, T. Fukumura, H. Toyosaki, M. Nakano, M. Kawasaki, *Appl. Phys. Lett.* **90**, 072103 (2007).
13. C. H. Ahn, J.-M. Triscone, J. Mannhart, *Nature* **424**, 1015 (2003).
14. See supporting material on *Science* Online.
15. S. J. Pennycook, L. A. Boatner, *Nature* **336**, 565 (1988).
16. C. L. Chien, C. R. Westgate, Eds., *The Hall Effect and Its Applications* (Plenum, New York, 1980).
17. J. T. Ye *et al.*, *Nat. Mater.* **9**, 125 (2010).
18. K. Ueno, H. Shimotani, Y. Iwasa, M. Kawasaki, *Appl. Phys. Lett.* **96**, 252107 (2010).
19. σ_{AH} is a suitable measure for an index of induced ferromagnetism. See supporting material on *Science* Online.
20. M. J. Calderón, S. Das Sarma, *Ann. Phys.* **322**, 2618 (2007) and references therein.
21. K. A. Griffin, A. B. Pakhomov, C. M. Wang, S. M. Heald, K. M. Krishnan, *Phys. Rev. Lett.* **94**, 157204 (2005).
22. M. Endo *et al.*, *Appl. Phys. Lett.* **96**, 022515 (2010).
23. D. Chiba, M. Yamanouchi, F. Matsukura, H. Ohno, *Science* **301**, 943 (2003).

Acknowledgments: Supported by Ministry of Education, Culture, Sports, Science and Technology of Japan KAKENHI grant 21019004 and by Funding Program for Next Generation World-Leading Researchers grant GR029.

Supporting Online Material

www.sciencemag.org/cgi/content/full/332/6033/1065/DC1
Materials and Methods
Figs. S1 to S3
Table S1
References (*24*–*27*)

23 December 2010; accepted 4 April 2011
10.1126/science.1202152

Downloaded from www.sciencemag.org on October 16, 2011